# Faraday Discussions

## Accepted Manuscript



Cite this: DOI: 10.1039/c0xx00000x

www.rsc.org/xxxxxx

ARTICLE

# Gold Nanowire Electrodes in Array: Simulation Study and Experiments

**Amélie Wahl, Karen Dawson, John MacHale, Seán Barry, Aidan J. Quinn and Alan O'Riordan***

***Received (in XXX, XXX) Xth XXXXXXXXX 20XX, Accepted Xth XXXXXXXXX 20XX***
**DOI: 10.1039/b000000x**

Recent developments in nanofabrication have enabled fabrication of robust and reproducible nanoelectrodes with enhanced performance, when compared to microelectrodes. A hybrid electron beam/photolithography technique is shown that permits discrete gold nanowire electrode arrays to be routinely fabricated at reasonable cost. Fabricated devices include twelve gold nanowire working electrode arrays, an on-chip gold counter electrode and an on-chip platinum pseudo reference electrode. Using potential sweep techniques, when diffusionally independent, these nanowires exhibit measurable currents in the nanoAmpere regime and display steady-state voltammograms even at very high scan rates (5000 $mV.s^{-1}$) indicative of fast analyte mass transport to the electrode. Nanowire electrode arrays offer the potential for enhancements in electroanalysis including: increased signal to noise ratio and increased sensitivity while also allowing quantitative detection at much lower concentrations. However, to achieve this goal a full understanding of the diffusion profiles existing at nanowire arrays is required. To this end, we simulate the effects of altering inter-electrode separations on analyte diffusion for a range of scan rates at nanowire electrode arrays, and perform the corresponding experiments. We show that arrays with diffusionally independent concentration profiles demonstrate superior electrochemical performance compared to arrays with overlapping diffusion profiles when employing sweep voltammetric techniques. By contrast, we show that arrays with diffusionally overlapping profiles exhibit enhanced performance when employing step voltammetric techniques.

## Introduction

Recent developments in fabrication of robust and reproducible nanoelectrodes have opened the door to a new and exciting area of electrochemistry[1, 2]. Typically these electrodes demonstrate enhanced performance, when compared to microelectrodes, due to improved mass transport occurring at the nanoelectrode thereby offering the potential for faster and more sensitive electroanalysis and improved kinetic measurement of electrochemical processes[3, 4]. Smaller electrode dimensions permit fabrication at higher densities on silicon chips enabling much greater-information gathering capability per device. Finally, nanoelectrodes typically exhibit shorter response times, lower RC constants, low analyte depletion and significantly reduced sample volumes[3].

To date, a significant portion of the studies employing nanoscale electrodes on silicon chips have been undertaken using nanodisks, nanopores or short inlaid nanobands[5]. However, large arrays of these structures are required to obtain reasonable measurable currents, i.e., in the nanoAmpere regime. By contrast, high aspect ratio nanostructures such as nanowires and nanobands, employed as electrochemical electrodes, exhibit relatively large currents (nA) due to the long length of the electrode (typically > 40 μm) but they also benefit from radial diffusion profiles to the electrode arising from their nanometre scale critical dimensions[3]. As such, these electrodes exhibit steady-state voltammograms indicative of fast analyte mass transport to the electrode even at very high scan rates (5000 $mV.s^{-1}$). Furthermore, advances in nanofabrication techniques pioneered by the micro/nanoelectronics industry including: electron beam, nanoimprint and phase-shift lithographies, have made fabrication and integration of robust and reproducible one dimensional (1-D) nanostructure-based devices routinely achievable at reasonable economic cost[6, 7].

Consequently, 1-D nanostructures have been employed to explore heterogeneous electron transfer rate constants with rates up to two orders of magnitude higher than previously measured being reported.[8-11] In addition, electrochemical devices employing discrete nanowire sensors demonstrating highly sensitive detection of key biomolecules including dopamine[7], hydrogen peroxide[12] and glucose[13] amongst others have recently been reported. Electrodes based on nanowire arrays offer the potential for further enhancements in electroanalysis including: increased signal to noise ratio and increased sensitivity while also allowing quantitative detection at much lower concentrations[14]. However, to achieve this goal, a full understanding of the diffusion profiles existing at nanowire arrays is required. During electron transfer processes, electroactive species around the electrode are depleted creating depletion zones known as Nernst diffusion layers, δ, which thickness varies considerably with the electrode dimensions and geometry. In sweep voltammetry a diffusion-limited and time-dependent response (planar diffusion) generally occurs with larger electrodes (e.g. macroelectrodes), while an ideal steady-state and time-independent response (radial diffusion) is typical of much smaller electrodes (e.g. ultramicroelectrodes)[3, 15].

At present, there is no analytical equation to describe diffusion to an electrode geometry where an electrode has sharp edges and protrudes from a planar substrate, i.e., a nanowire. For this reason, analytical solutions based on similar geometries such as hemicylinders or nanobands have been proposed and adopted to estimate voltammetric/mass transport behaviour at nanowire electrodes[16]. In this regard, the thickness of a Nernst diffusion layer, $\delta$, at a hemicylindrical electrode approaching steady-state conditions can be estimated via the following equation:

$$\delta = r_0 \left( \ln \frac{2(\mathrm{D_O} t)^{\frac{1}{2}}}{r_0} \right) \quad \textbf{(1)}$$

where $D_O$, is the diffusion coefficient, $t$ is time and $r_0$ is the electrode radius. For a nanowire $r_0 = w/4$ where, $w$ is the width of the electrode[16-18]. In this manner diffusion independence is theoretically maintained by ensuring that the separation between neighbouring electrodes, $s$, is greater than twice the diffusion thickness ($s > 2\delta$). However, we and others have recently shown that this is not the case at the nanoscale and significantly larger separations are required to maintain diffusional independence between neighbouring electrodes and this separation is significantly affected by applied scan-rate [14, 19].

In this work, we undertake finite element analysis of diffusion profiles existing at arrays of nanowire electrodes (Comsol Multiphysics) and explore the effects of altering inter-electrode separations on diffusional independence for a range of scan rates. Although a range of scan rates are modelled, we are particularly interested in very high scan rates (5000 $mV.s^{-1}$) since this allows rapid (sub 1 second) data capture required for ,e.g., biomedical, environmental and pharmaceutical diagnostic applications. To confirm our simulations experimentally, electron beam lithography, metal evaporation and lift-off techniques were employed to fabricate fully integrated nanowire array devices on silicon chips. These devices are fabricated in a manner as to include on-chip counter and pseudo reference electrodes. Finally, we show that arrays that are diffusionally independent demonstrate superior electrochemical performance when employing sweep voltammetric techniques compared to arrays with overlapping diffusion profiles. By contrast, arrays with diffusionally overlapping profiles exhibit enhanced performance when employing step voltammetric techniques.

## Experimental

### Finite-Element Simulations

Analyte concentration profiles for the oxidation of a redox molecule at electrode arrays containing three nanowires are simulated using the commercial finite element software package Comsol Multiphysics 4.1. (COMSOL, SE). These simulations are based on the single electron oxidation process of FcCOOH in solution at the nanowire electrodes surface, corresponding to:

$$\mathrm{O} + e^- = \leftrightharpoons \mathrm{R} \quad \textbf{(2)}$$

The objective of these simulations is to assess the distance required between adjacent nanowires in array to allow independent diffusional mass transport to each nanowire electrodes when in array, at high scan rates. As electrochemical experiments are undertaken in presence of excess supporting electrolyte, in static un-agitated environments at constant temperature and over short time periods, mass transport effects arising from migration and convection are assumed to be negligible. Thus emphasis is put on diffusional mass transport alone and only Fickian diffusion to a nanoband electrode in two dimensions is considered [18, 19]:

$$\frac{\partial C_\mathrm{i}}{\partial t} = D_i \left( \frac{\partial^2 c_i}{\partial x^2} + \frac{\partial^2 c_i}{\partial y^2} \right) \quad \textbf{(3)}$$

where $C_i$ and $D_i$ represent the concentration and diffusion coefficient of the redox species in solution, respectively. In these models, the redox analyte concentration is 1 mM FcCOOH in 10 mM PBS, with an associated diffusion coefficient of 5.4 x $10^{-6}$ $cm^2.s^{-1}$ [20]. Given the electron transfer process is reversible, both species O and R are soluble in solution and their diffusion coefficients are assumed to be equal ($D_O = D_R$), the concentration of FcCOOH (species R) at the nanowire electrodes surface at a given time interval for a potential sweep method may be expressed by the following Nernstian boundary conditions [4, 18]:

at t = 0:
$$C_R(\mathrm{t}) = C_R^* \quad \textbf{(4)}$$

at t > 0:
$$C_R(\mathrm{t}) = \frac{C_R^*}{1 + \exp\left[\frac{nF}{RT}\left(E^0 - E(\mathrm{t})\right)\right]} \quad \textbf{(5)}$$

where $t$ is time (s), $C_R^*$ and $C_R(\mathrm{t})$ are concentration ($mol.m^{-3}$) of the reductant species $R$ in the bulk, and at the electrode surface with respect to time respectively, $n$ is the number of electrons exchanged, $F$ is Faraday's constant (96485 $C.mol^{-1}$), $R$ is the gas constant (8.314 $J.mol^{-1}.K^{-1}$), $T$ is temperature (K), $E_0$ is the formal potential of the redox couple (V). $E$(t) is the applied potential (V) defined as:

$$E(\mathrm{t}) = E_{int} + \upsilon \mathrm{t} \quad \textbf{(6)}$$

where $E_{int}$ is the initial voltage (V) of the potential sweep and $\upsilon$ is the scan rate ($V.s^{-1}$). From experimental results, a value of 0.155 V is used for $E_0$ and simulations are carried out in a potential window of -0.15 to 0.45 V for scan rates of 20, 100 and 5000 $mV.s^{-1}$.

### Nanowire Fabrication

Gold nanowire array electrodes are fabricated using a hybrid electron beam/photo-lithography process on four inch wafer silicon substrates bearing a ~300 nm layer of thermally grown silicon dioxide ($Si/SiO_2$). In this approach, nanowires and alignment marks are patterned in resist (ZEP 520 Nippon Zeon) by direct electron beam writing (50 kV beam voltage, 100 pA beam current and 120 μC.cm-2 beam dose). Following resist

development, gold layers (Ti/Au 5/50 nm) are blanket deposited by metal evaporation (Temescal FC-2000 E-beam evaporator) and removed from un-patterned areas using standard lift-off techniques to yield nanowire stacked structures. Using electron beam written alignment marks, interconnection tracks are then overlaid onto nanowires termini by optical lithography, metal evaporation (Ti/Au 10/90 nm) and lift-off. Peripheral electrical contact pads, interconnection tracks and two central half-disk gold electrodes (all Ti/Au 10/90 nm) are deposited using the same procedure. A further metal deposition (Ti/Pt 10/90 nm) step is then performed onto one half-disk electrode. In this manner, the central half-disk electrodes may be employed as a gold counter and platinum pseudo reference electrode, respectively.

To prevent unwanted electrochemical reactions occurring between metal interconnection tracks and electrochemically active species, a silicon nitride passivation layer (~500 nm) is then deposited by plasma-enhanced chemical vapour deposition (PECVD) onto the wafer surface. Photolithography and dry etching are then employed to selectively open windows (~45 x 100 μm) in the passivation layer directly above the gold nanowire working electrodes to allow exclusive contact between them and an electrolytic solution. Openings are also maintained above the counter, and reference electrodes along with peripheral contact pads. Following fabrication, wafers are diced into 16 x 16 mm chips. Each chip contains twelve individually contacted gold nanowire working electrode arrays, an integrated gold counter electrode and a platinum pseudo-reference electrode.

**Structural and Electrical Characterisation:**

Optical micrographs of nanowire electrode arrays are acquired using a calibrated microscope (Axioskop II, Carl Zeiss Ltd.) equipped with a charge-coupled detector camera (CCD; DEI-750, Optronics). Structural characterisation is undertaken using scanning electron microscopy (SEM); images captured using a field emission SEM (JSM-6700F, JEOL UK Ltd.) operating at beam voltages between 5 and 10 kV. As a quality control check, to confirm electrical functionality, two-point electrical measurements are performed using a probe station (Model 6200, Micromanipulator Probe Station) in combination with a source meter (Keithly 2400) and a dedicated LabVIEW$^{TM}$ V8.0 program. In these current-voltage (I-V) measurements, the source electrode is grounded, a bias sweep up to ± 10 mV is applied to the drain electrode, and the current through the nanowire is measured.

**Electrochemical analysis**

All electrochemical studies are performed using a CHI660a Electrochemical Analyzer and a Faraday Cage CHI200b (CH Instruments) connected to a PC. All experiments employ a standard three-electrode cell configuration using gold nanowire arrays as the working electrodes, versus the on-chip gold counter electrode and on-chip platinum pseudo-reference electrode. Cyclic voltammetry (CV) is conducted in 10 mM phosphate buffer saline (PBS, pH 7.4) and in 1 mM ferrocenemonocarboxylic acid (FcCOOH) in 10 mM PBS in the voltage range of -0.15 V to 0.45, for a variety of scan rates (5, 10, 20, 50, 100, 200, 500, 1000, 2000 and 5000 mV.s$^{-1}$). Square wave voltammograms are undertaken in 0.1 to 5 mM FcCOOH in 10 mM PBS solutions and in 10 mM PBS only in the voltage range of -0.15 to 0.45 V with an incremental potential of 0.001 V, a potential amplitude of 0.025 V and a frequency of 25 Hz. All chemicals are purchased from Sigma Aldrich and used as received. All solutions are freshly prepared using deionized water (18.2 MΩ.cm, ELGA Pure Lab Ultra). Prior to electrochemical experiments, all electrodes are cleaned by sequential immersion for 10 minutes in acetone, trichloroethylene, , iso-propyl alcohol, followed by a thorough rinse with deionized water and dried in stream of nitrogen.

## Results and discussion

Due to the high aspect ratio of the nanowires within an array, a simplified two dimensional model known as the diffusion domain approach is adopted[15, 19]. To perform simulations, a cross sectional plane through an array comprising of three nanowires is defined where each nanowire electrode within an array is assigned its own area; see Figure 1 (a). In this manner, each nanowire is outlined by a 50 nm x 100 nm rectangle (height x width) located centrally at the bottom of a much larger rectangle (space domain). To ensure accuracy of the simulations, the domain area is selected so as to be large enough to ensure bulk-like conditions at the boundaries remain unaffected by the electrochemistry occurring at the electrodes. Figure 1 (b) depicts the two-dimensional geometry of the model employed with boundary conditions for flux = 0 and for concentration of the reductant species R in the bulk and at the electrode surface with respect to time, respectively $C_R^*$ and $C_R(t)$. During simulations the mesh is duly refined and simulations are allowed to iteratively resolve until a convergence error less than 2% is achieved.

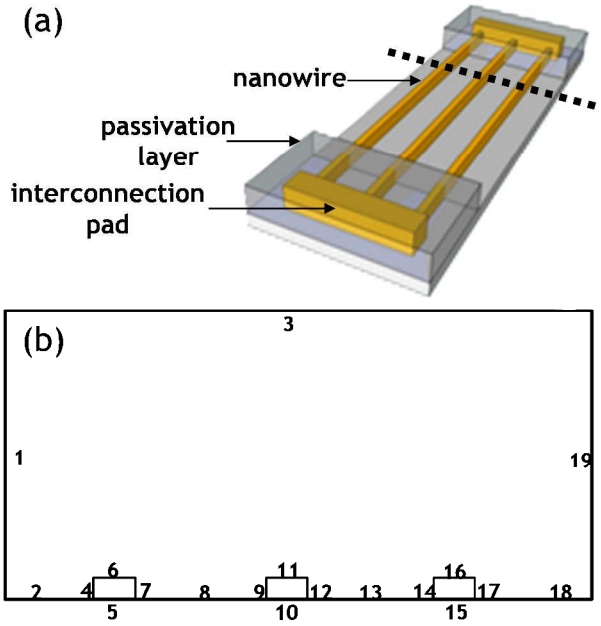


Figure 1: (a) Schematic diagram of three nanowire electrodes in array. (b) 2D representation of three nanowire electrodes in array, used for simulation of diffusion at nanowire electrodes. Boundaries 1, 3 & 19 define the bulk concentration, $C^*$. Boundaries 2, 8, 13 & 18 correspond to flux = 0. No conditions are applicable at boundaries 5, 10 & 15. Boundaries 4, 6, 7, 9, 11, 12, 14, 16, & 17 are the concentration present at the electrode surface with respect to the time step of the electrolysis.

We have previously demonstrated that radial diffusion of 1 mM FcCOOH in 10 mM PBS occurs at single gold nanowire electrodes (50 nm high, 100 nm wide and 45 µm long) using cyclic voltammetry for scan rates ranging from 20 $mV.s^{-1}$ to 5000 $mV.s^{-1}$.[3] At electrode arrays, the inter-electrode separation is the critical factor that determines whether diffusional profiles overlap when other parameters including: electrode width, solution composition (buffer type, concentration, etc.) and scan rate are kept constant. In this work, arrays containing three nanowires are chosen as they contain only one inner electrode competing for diffusional species on either side. Models are built for arrays with increasing nanowire electrodes separations, i.e., 5, 10, 15 and 20 µm for which diffusion profiles using 1 mM FcCOOH in 10 mM PBS under cyclic voltammetric conditions are calculated. The nanowire dimensions are maintained as 100 nm in width and 50 nm in height with $D_R$ = 5.4 x $10^{-6}$ $cm^2.s^{-1}$, $E^0$ = 0.155 V, $T$ = 298.15 K. As can be clearly seen in Figure 2 (a) and (b) overlap of adjacent diffusion layers occurs for nanowire arrays with inter-electrode separation of 5 and 10 µm. By comparison, in Figures 2 (c) and (d), for an inter-electrode distance of 15 and 20 µm, the diffusion layers at each electrode in the array are completely independent from each other and radial in shape, suggesting that each electrode in the array should behave as an individual electrode and that the current response of the whole array should be equivalent to three times that of a single nanowire.

To confirm simulation results, gold nanowire arrays are fabricated using a hybrid electron beam/photo-lithography process at $Si/SiO_2$ substrates as described in the experimental section. Following fabrication, each electrodes are structurally characterised using optical microscopy and SEM. Figure 3 (a) shows an optical micrograph of a gold counter electrode (left) and pseudo-reference platinum electrode (right) integrated at a chip surface. An optical image of a fully fabricated, integrated and passivated single nanowire device is shown in Figure 3 (b). The gold squares at both nanowire termini are defined during the electron beam lithography step to minimise contact resistance when overlaid by the metallic interconnection tracks.

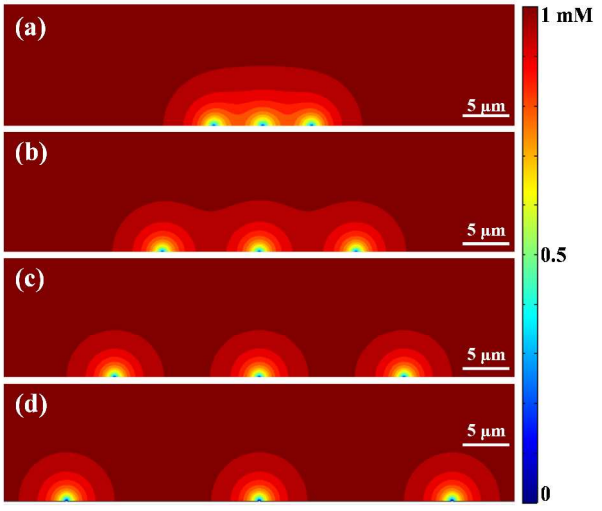


Figure 2: 2D simulations of FcCOOH concentration profiles at three nanowire arrays separated by: (a) 5 µm, (b) 10 µm, (c) 15 µm and (d) 20 µm at 5000 $mV.s^{-1}$..

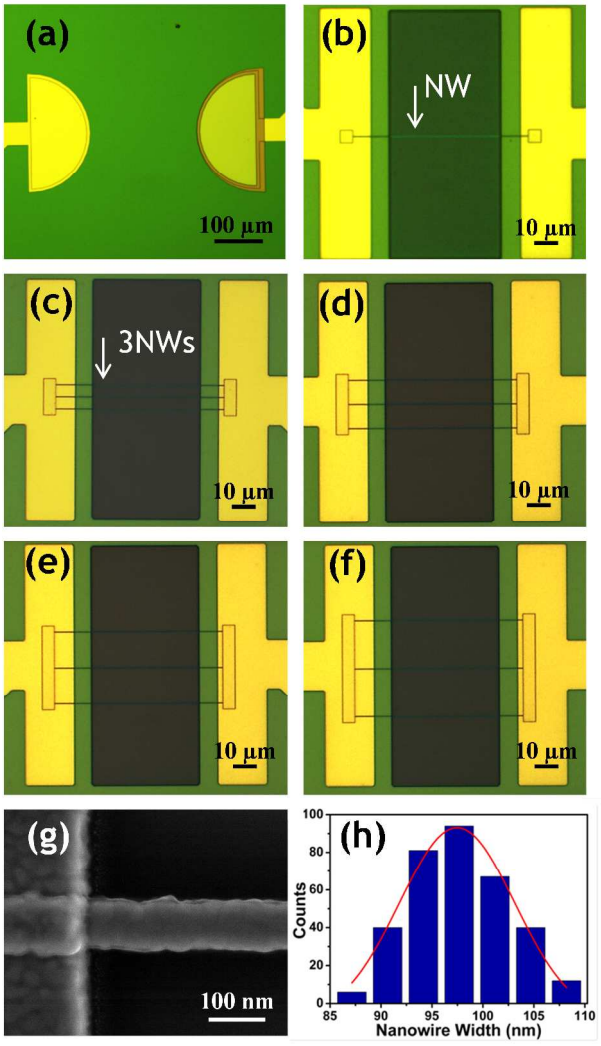


**Figure 3:** Optical micrographs of fully integrated and passivated (a) gold counter (left) and platinum reference electrodes (right), (b) single gold nanowire electrode. Nanowire electrode arrays containing three nanowires separated by (c) 5 µm, (d) 10 µm, (e) 15 µm and (f) 20 µm. The darker rectangle in the middle corresponds to the trench selectively opened in silicon nitride above the nanowires to allow contact with an electrolyte solution. (g) High magnification SEM micrograph of a region of passivated and fully exposed nanowire. (h) Histogram showing the distribution of widths of nanowires obtained from SEM analysis. Solid red line is a Gaussian fit to the data.

Figures 3 (c) to (f) are optical micrographs of fully fabricated, integrated and passivated three nanowire electrodes in array separated by 5, 10, 15 and 20 µm, respectively. The gold bars at the nanowire termini are again employed to minimise contact resistance. The width of the passivation window (central dark rectangle) defines the exposed nanowire length at 45 µm for both single nanowires and nanowire arrays. Visual inspection using SEM microscopy reveals excellent registration between nanowire electrodes and the overlaid micron-scale interconnection tracks, ensuring nanowires are well electrically contacted and uniform in width; see Figure 3 (g). A statistical analysis at multiple locations across seventeen individual nanowire structures (n=

340) from different chips yielded an average nanowire width of ~ 98 ± 5 nm (variation of ~5.1%), as presented in Figure 3 (h). This confirmed that proximity effects did not arise during the electron beam lithography process and consequently nanowire broadening did not occur.

Nanowire electrode devices were electrically characterised using standard two-point *I-V*, see supplementary information. All functioning nanowire array devices display linear Ohmic responses confirming good electrical contact to nanowires by the interconnections tracks, see Figure S1.

CV experiments corresponding to the simulations presented in Figure 2 are performed by applying a potential range of -0.15V to 0.45V to nanowire arrays in 1 mM FcCOOH in 10 mM PBS, pH 7.4, at 5000 $mV.s^{-1}$. Typical CVs obtained for arrays with electrode separations of 5 µm and 15 µm are shown in Figure 4.

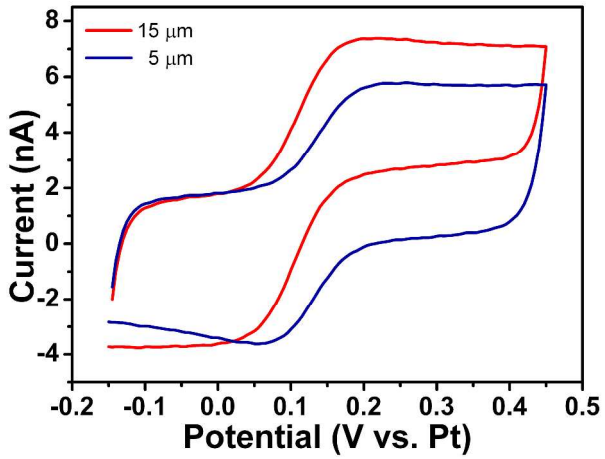


**Figure 4**: Cyclic voltammograms obtained at 5000 $mV.s^{-1}$ scan rate in 1 mM FcCOOH in 10 mM PBS at arrays comprising three nanowires separated by 5 and 15 µm.

The forward sweep of the 5 µm spaced array exhibits steady-state behaviour, however, a diffusive peak is evident on the return reduction sweep indicative of diffusional overlap which is in agreement with the simulation results. By contrast both the forward and backward sweeps of the 15 µm spaced array exhibit steady-state behaviour also in agreement with the simulation results. These data strongly suggesting that these electrodes are fully diffusionally independent. This is further supported by the observed increase in measured faradaic peak current $I_p$ = 5.26 nA for 15 µm spaced arrays compared with $I_p$ = 3.12 nA for the 5 µm spaced arrays, an increase of ~60%. The magnitude of the steady-state currents for all nanoelectrodes devices are found to be highly reproducible for measurements from separate nanowire arrays on different chips (n=15 for each array). The magnitude of the average steady-state current measured at nanoelectrodes separated by 5 µm, 5.9 ± 0.2 nA, is the same (within experimental error) to the average measured at nanoelectrodes separated by 10 µm, 6.2 ± 0.3 nA (data not shown), while the magnitude of the average currents measured for nanoelectrode arrays separated by 15 µm and 20 µm, is 7.0 ± 0.5 nA and 6.9 ± 0.3 nA (data not shown), respectively is again the same within experimental error. It is therefore likely that this increase in observed current measured for the latter two arrays arises from improved mass transport occurring at diffusion independent electrodes. At low scan rates (5 $mV.s^{-1}$) all nanowire arrays exhibit steady-state behaviour with very low hysteresis is observed between the forward and reverse sweeps of the CVs (data not shown).

Steady-state CVs allow kinetic information for an electronic transfer process occurring at an electrode surface such as the heterogeneous rate of electron transfer $k_0$ to be determined. Historically, experiments undertaken to determine $k_0$ using macro and ultra-microelectrodes have been diffusion limited as such that low values have been reported.[8-11] The advent of nanoscale electrodes have eliminated diffusion effects and permitted higher (truer) values to be experimentally determined [21].

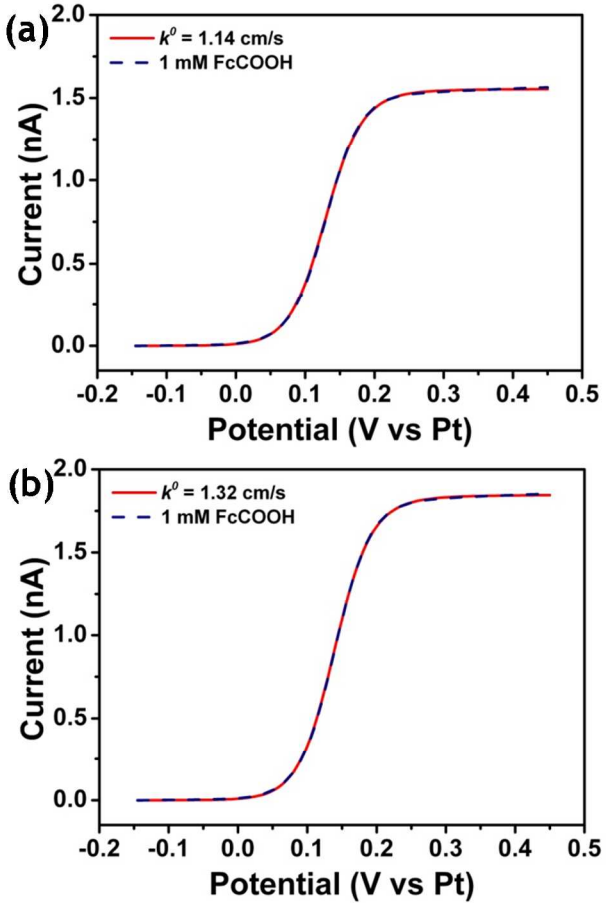


**Figure 5**: Fits of Butler-Volmer kinetic equation to an experimental cyclic voltammogram obtained for a single electron oxidation of FcCOOH at 5 $mV.s^{-1}$ at three nanowire electrodes separated by (a) 5 µm and (b) 15 µm. In both cases $R^2$ = 0.999.

To explore how much diffusional overlap may affect the extraction of the heterogeneous rate of electron transfer, we employed a three parameter fit to extract the $k_0$ values from cyclic voltammograms obtained using nanowire arrays (5 $mV.s^{-1}$) separated by 5 µm and 15 µm, respectively.

The steady-state voltammogram of an uncomplicated quasi-reversible one-electron oxidation reaction may be expressed by Butler-Volmer type kinetics [12, 21]:

$$i_{bv} = \frac{i_{mt}}{1+\exp\left[\frac{-F\left(E-E^{0'}\right)}{RT}\right]+\frac{m}{k^0}\exp\left[\frac{-F(1-\alpha)\left(E-E^{0'}\right)}{RT}\right]} \quad (7)$$

where $i_{mt}$ is the mass transfer diffusion-limited current, $F$ is the Faraday constant, $R$ is the molar gas constant, T is temperature (K), $E$ is the applied potential, $E_0'$ is the formal potential of the redox-couple, $\alpha$ is the transfer coefficient, $k^0$ is the standard heterogeneous rate constant (cm.s$^{-1}$) and $m$ is the mass transfer coefficient (cm.s$^{-1}$). Equation (7) involves the assumption of identical diffusion coefficients of the oxidized and reduced species and a uniformly accessible electrode surface. The mass transfer coefficient may then be expressed as $m=i_{mt}(AFC)^{-1}$, where $A$ is the electrode surface area and $C$ is the bulk concentration of the electroactive species. Non-linear least square fitting of experimental voltammograms by Equation (7) was performed by the Levenberg-Marquardt algorithm using $k^0$, $\alpha$, and $i_{mt}$ as fitting parameters; see Figure 5. The other parameters in equation 7 were fixed at; $E^{0'}$ = 0.155 V, $C$ = 1 mM and $A$ = 2.7 x 10$^{-7}$ cm$^2$ (3 times the geometric area of a single nanowire). Equation (7) provides an excellent description of both experimental curves. This fits yielded k$^0$ values of 1.14 ± 0.03 cm.s$^{-1}$ and 1.32 ± 0.03 cm.s$^{-1}$ for 5 µm and 15 µm spaced electrodes, respectively with correlations of R$^2$ = 0.999 for both fits; see Figure 6. This latter value is in excellent agreement to the values determined using single (diffusionally independent) nanowires 1.29 ± 0.03 cm.s$^{-1}$ [3] confirming the diffusional independent nature of the 15 µm spaced arrays. In comparison, the value of 1.14 ± 0.03 cm.s$^{-1}$ is ~12 % lower, which confirms the presence of diffusional overlap at 5 µm spaced arrays.

In square wave voltammetry, molecules are repeatedly oxidised and reduced as the voltage is stepped positively and negatively (in the appropriate voltage range, frequency etc.).[22-25] During this process, molecules continuously diffuse to and from an electrode surface. Diffusion thereby limits the achievable signal as oxidised (or reduced) molecules diffuse from the electrode prior to being reduced (or oxidised). It is hypothesised that by fabricating nanowire arrays with overlapping diffusion profiles, molecules oxidised (reduced) at one nanowire may diffuse to a neighbouring nanowire within an array (rather than to bulk solution) where it may consequently be reduced (oxidised) during a subsequent voltage step. This approach should result in increased signal to noise and consequently sensitivity in direct contrast with sweep voltammetry.

To confirm this hypothesis, square wave voltammetric measurements were undertaken for FcCOOH concentrations ranging from 0.1 mM to 5 mM in 10 mM PBS. Figure 6 (a) shows typical square wave voltammograms recorded for 5 mM FcCOOH at (i) a single nanowire electrode, (ii) nanowire electrode arrays separated by 5 µm and (iii) nanowire electrode arrays separated by 15 µm. All recorded signals display current peaks in the voltage range of 0.15 to 0.20 V vs. the on-chip Pt pseudo-reference electrode. Clearly an increase in measured current signal is observed when increasing the number of nanowires from one to three within an array; (i) versus (ii) & (iii) in Figure 6. Of note, is that a further increase in signal is observed when the inter-electrode separation is decreased from 15 µm (iii) to 5 µm (ii) confirming that diffusionally overlapped nanoelectrode arrays provide higher signal to noise than diffusionally independent variants. Figure 6 (b) shows the calibration plots obtained for FcCOOH concentrations ranging from 0.1 mM to 5 mM in 10 mM PBS for the single nanowire (i) and for the two different nanowire electrode arrays (ii) & (iii) as described above. These results are important to nanoscale electroanalysis as they suggest that a 'design for application' approach should be adopted prior to electrode fabrication in order to maximise sensitivity. Consequently this requires either *a priori* knowledge or at least a good appreciation of the diffusion regimes present at nanowire electrodes.

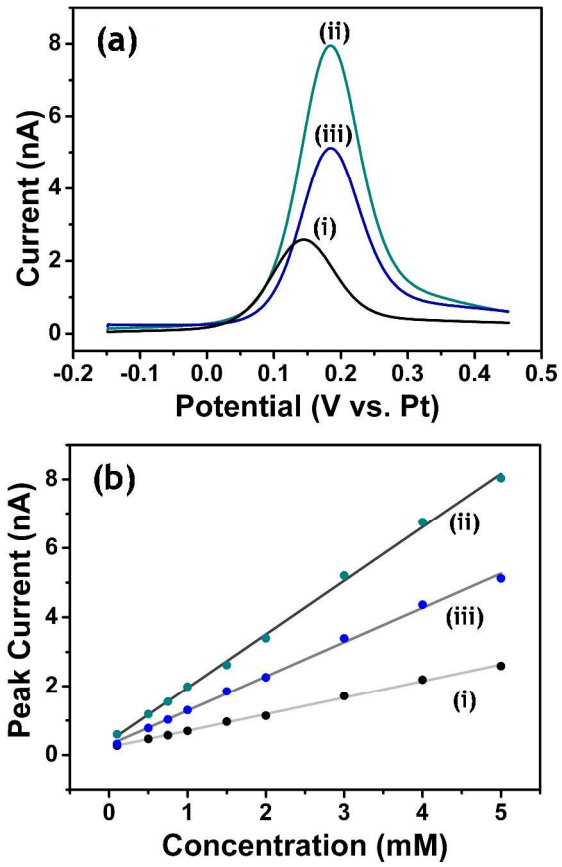


**Figure 6:** (a) Typical square wave voltammograms of 5 mM FcCOOH in 10 mM PBS at (i) a single nanowire electrode, (ii) three nanowire electrodes array separated by 5 µm and (iii) three nanowire electrodes array separated by 5 µm. (b) Corresponding calibration plots for a range of FcCOOH concentrations 0.1, 0.5, 0.75, 1, 1.5, 2, 3, 4 & 5.mM in 10 mM PBS, R2 = 0.999.

## Conclusions

We show a hybrid electron beam/photolithography technique that permits gold nanowire array electrodes to be routinely fabricated at reasonable cost. Nanowire electrode arrays offer the potential for enhancements in electroanalysis including: increased signal to noise ratio and increased sensitivity while also allowing quantitative detection at much lower concentrations. However, to achieve this goal a full understanding of the diffusion profiles

existing at nanowire arrays would be required. To this end, we simulated the effects of altering inter-electrode separations on analyte diffusion for a range of scan rates at nanowire electrode arrays and we confirmed these results experimentally. Fabricated devices include twelve gold nanowire working electrode arrays, an on-chip gold counter electrode and an on-chip platinum pseudo reference electrode. CVs undertaken using these nanowire arrays exhibit measurable currents in the nanoAmpere regime and display steady-state voltammograms even at low scan rates (5 mV.s-1) indicative of fast analyte mass transport to the electrode. We show that arrays that are sufficiently spaced so that they have diffusionally independent concentration profiles demonstrate superior electrochemical performance when employing sweep voltammetric techniques compared to arrays with overlapping diffusion profiles. By contrast, we also show that arrays with diffusionally overlapping profiles exhibit enhanced performance when employing step voltammetric techniques, e.g., square wave voltammetry. These results show that, to optimise sensitivity in nanoscale electroanalysis the final application needs to be taken into account when initially designing nanoscale electrode arrays.

## Acknowledgements

The authors would like to thank the engineers of the Tyndall Central Fabrication Facility in particular, Mr D O'Connell, Mr B McCarthy, and Mr V. Djara for their assistance and advice. This work was supported by Science Foundation Ireland under the Research Frontiers Programme (SFI/09/RFP/CAP2455), by the European Commission under the FP7 Security Project CommonSense (261809) and FP7 ICT project "Nanofunction" (257375) and the Irish Higher Education Authority PRTLI programs (Cycle 3 "Nanoscience" and Cycle 4 "INSPIRE").

## Notes and references

*Tyndall National Institute – University College Cork, Lee Maltings, Dyke Parade, Cork, Ireland. Tel:+353 21 2346403. alan.oriordan@tyndall.ie.*

† Electronic Supplementary Information (ESI) available: [details of any supplementary information available should be included here]. See DOI: 10.1039/b000000x/

1. Shao, Y.H., et al., *Nanometer-sized electrochemical sensors.* Analytical Chemistry, 1997. **69**(8): p. 1627-1634.
2. Conyers, J.L. and H.S. White, *Electrochemical characterization of electrodes with submicrometer dimensions.* Analytical Chemistry, 2000. **72**(18): p. 4441-4446.
3. Dawson, K., et al., *Electroanalysis at Single Gold Nanowire Electrodes.* Journal of Physical Chemistry C, 2012. **116**(27): p. 14665-14673.
4. Guerrette, J.P., S.J. Percival, and B. Zhang, *Voltammetric Behavior of Gold Nanotrench Electrodes.* Langmuir, 2011. **27**(19): p. 12218-12225.
5. Murray, R.W., *Nanoelectrochemistry: Metal nanoparticles, nanoelectrodes, and nanopores.* Chemical Reviews, 2008. **108**(7): p. 2688-2720.
6. Menke, E.J., et al., *Lithographically patterned nanowire electrodeposition.* Nature Materials, 2006. **5**(11): p. 914-919.
7. Tyagi, P., et al., *Patternable Nanowire Sensors for Electrochemical Recording of Dopamine.* Analytical Chemistry, 2009. **81**(24): p. 9979-9984.
8. Antiochia, R., et al., *Single-wall carbon nanotube paste electrodes: a comparison with carbon paste, platinum and glassy carbon electrodes via cyclic voltammetric data.* Electroanalysis, 2004. **16**(17): p. 1451-1458.
9. Zhang, Y., et al., *Determination of electrochemical electron-transfer reaction standard rate constants at nanoelectrodes: Standard rate constants for ferrocenylmethyltrimethylammonium(III)/(II) and hexacyanoferrate(III)/(II).* Electroanalysis, 2008. **20**(13): p. 1490-1494.
10. Watkins, J.J., et al., *Zeptomole voltammetric detection and electron-transfer rate measurements using platinum electrodes of nanometer dimensions.* Analytical Chemistry, 2003. **75**(16): p. 3962-3971.
11. Watkins, J.J. and H.S. White, *The role of the electrical double layer and ion pairing on the electrochemical oxidation of hexachloroiridate (III) Pt electrodes of nanometer dimensions.* Langmuir, 2004. **20**(13): p. 5474-5483.
12. Dawson, K., et al., *Single Nanoskived Nanowires for Electrochemical Applications.* Analytical Chemistry, 2011. **83**(14): p. 5535-5540.
13. Dawson, K., M. Baudequin, and A. O'Riordan, *Single on-chip gold nanowires for electrochemical biosensing of glucose.* Analyst, 2011. **136**(21): p. 4507-4513.
14. Dawson, K., et al., *Electroanalysis at discrete arrays of gold nanowire electrodes.* Electrochimica Acta, (0).
15. Davies, T.J. and R.G. Compton, *The cyclic and linear sweep voltammetry of regular and random arrays of microdisc electrodes: Theory.* Journal of Electroanalytical Chemistry, 2005. **585**(1): p. 63-82.
16. Wightman, R.M. and D.O. Wipf, *Voltammetry At Ultramicroelectrodes.* Electroanalytical Chemistry, 1989. **15**: p. 267-353.
17. Bard, A.J., L.R., Faulkner, . Electrochemical Methods, Fundamentals & Applications, 2011(Second ed.; Wiley & Sons.,: New York.).
18. Molina, A., et al., *Voltammetry of Electrochemically Reversible Systems at Electrodes of Any Geometry: A General, Explicit Analytical Characterization.* Journal of Physical Chemistry C, 2011. **115**(10): p. 4054-4062.
19. Godino, N., et al., *Mass Transport to Nanoelectrode Arrays and Limitations of the Diffusion Domain Approach: Theory and Experiment.* Journal of Physical Chemistry C, 2009. **113**(25): p. 11119-11125.
20. Zoski, C.G., *Handbook of Electrochemistry.* Handbook of Electrochemistry; 1st Edition ed.; Elsevier: Oxford, 2007.Elsevier: Oxford, 2007(1st Editioned).
21. Heller, I., et al., *Individual single-walled carbon nanotubes as nanoelectrodes for electrochemistry.* Nano Letters, 2005. **5**(1): p. 137-142.
22. Whelan, D.P., et al., *SQUARE-WAVE VOLTAMMETRY AT SMALL DISK ELECTRODES - THEORY AND EXPERIMENT.* Journal of Electroanalytical Chemistry, 1986. **202**(1-2): p. 23-36.

23. Odea, J., et al., *SQUARE-WAVE VOLTAMMETRY AT ELECTRODES HAVING A SMALL DIMENSION*. Analytical Chemistry, 1985. **57**(4): p. 954-955.
24. Osteryoung, J.G. and R.A. Osteryoung, *SQUARE-WAVE VOLTAMMETRY*. Analytical Chemistry, 1985. **57**(1): p. A101-&.
25. Ramaley, L. and M.S. Krause, *THEORY OF SQUARE WAVE VOLTAMMETRY*. Analytical Chemistry, 1969. **41**(11): p. 1362-&.